Mechanics & Industry **21**, 415 (2020)
© AFM, EDP Sciences 2020
https://doi.org/10.1051/meca/2020046

Mechanics & Industry

Available online at:
www.mechanics-industry.org

Regular Article

FEM based mathematical modelling of thrust force during drilling of Al7075-T6

Anastasios Tzotzis[1,*], César García-Hernández[1], José-Luis Huertas-Talón[1], and Panagiotis Kyratsis[2]

[1] Department of Design and Manufacturing Engineering, University of Zaragoza, 50018, Zaragoza, Spain
[2] Department of Industrial Design Engineering, University of Western Macedonia, 50100, Kila Kozani, Greece

Received: 12 March 2020 / Accepted: 28 May 2020

Abstract. Like most machining processes, drilling is affected by many parameters such as the tool diameter, the cutting speed and feed. The current research investigates the possibility of developing a finite element modelling based prediction model for the generated thrust force during drilling of Al7075-T6 with solid carbide tools. A total of 27 drilling experiments were carried out in order to examine the interaction between three key parameters and their effect on thrust force. In addition, simulations of the experiments were realized with the use of DEFORM3D™ software in order to obtain the necessary numerical data. Finally, a comparison was made between the experimental and the numerical results to verify that reliable modelling is feasible. The mathematical model was acquired with the use of response surface methodology and the verification of the adequacy of the model was performed through an analysis of variance. The majority of the simulations yielded results in agreement with the experimental results at around 95% and the derived model offered an accuracy of 5.9%.

Keywords: al7075 drilling / finite element method / deform3d / response surface methodology / thrust force

1 Introduction

As technology advances, manufacturing industries tend to design products with parts that require machining with the highest standards available and at the lowest possible cost. Such optimization during the manufacturing stage of a product, require a lot of early planning and thorough research, which lead to increase development time and cost. In order to reduce these factors during the development stage, the implementation of finite element method (FEM) and similar techniques are widely applied.

An early example of FEM in machining is the work completed by Klamecki [1] that was published in 1973. Since then, as the computational resources advance, more and more researchers took advantage of FEM in machining. Drilling is one of the most used metal cutting operations, which can benefit from the use of FEM. Due to the fact that drilling is an intricate process, with complex tool and chip geometries, it was included to commercial FEM software in the last few years. Guo and Dornfeld [2] developed a nonlinear 3D finite element model which considers thermal, elastic and plastic parameters to study burr formation in drilling of 304L stainless steel. Similarly, 3D FEM of chip formation during drilling is another topic that is widely studied [3–6]. Chip formation progress, chip thickness, burr height and surface roughness are some of the parameters that are discussed. FEM is used for prediction purposes as well. 3D models and computational methods are used for measuring and predicting important parameters such as thrust force and torque [4,7,8]. In addition to the aforementioned parameters, temperature of the tool-workpiece interface is another important property that can be measured with the aid of finite element (FE) models, in order to develop methods for tool wear prediction and cutting parameters optimization [9,10].

Since metal materials are very common in manufacturing industries, such as aerospatial, automotive and machinery, most studies related in these areas focus on materials like titanium alloys, aluminium alloys and carbon steels. Davim and Maranhão [11] utilized a finite element analysis for examination purposes. Plastic strain and plastic strain rate during the process of machining AISI 1020 steel were the main assessed parameters during their study. Additionally, authors validated the process using experimental values from literature and verified that simulated results were close to the ones found in literature. Belis et al. [12] used the finite element method for the determination of the developed stresses along the cutting edges of a twist drill, while the cutting forces have been

* e-mail: atzotzis@unizar.es

already calculated using a CAD based approach. Lotfi et al. [13] investigated the drilling process of AISI1045 and developed a 3D FE model for prediction purposes of the produced heat and flank wear on the drill by using a modified Usui model.

Parida [14] investigated the evaluation of several properties like torque, thrust force, strain and temperature on drills, with the aid of 3D FE modelling for Ti-6Al-4V alloy. In addition, he experimentally validated the results. Similarly, Nagaraj et al. [15] used DEFORM3D™ to develop a FE based model to simulate the thrust force, stress, strain and temperature at the tool's cutting edge when drilling Nimonic C-263 alloy. Dou et al. [16] worked on a new constitutive model, to improve a prediction model for thrust force and torque. Moreover, authors tested the efficiency of their constitutive model by using finite element modelling for simulating the drilling process of SiCp/Al6063.

Especially for drilling of aluminum alloys of the 7000 series, even though many studies exist in the literature that present experimental analysis of Al7075 drilling [17–19], the number of studies that implement FE models is still low. A study on the thermal and mechanical behavior of aluminum alloys (Al 7075-0) during machining with PCD (polycrystalline diamond) and cemented carbide tools was made by Davim et al. [20]. Additionally, they compared the performances of both tools. Similarly, Ucun [21] emphasized with his study the advantages that arise when 3D modelling the metal cutting processes and examined the performances of the twist and 3-flute drills. The performance of the drills was assessed focusing on the generated thrust force, torque and stress. Sahu and Andhare [22] presented in their work a prediction model using response surface methodology (RSM) for determining the residual stress that occurs when turning Ti-6Al-4V, assisted by 3D FEM and experiments.

With these in mind, the present paper contributes towards both an experimental and a 3D numerical study on drilling of Al7075-T6, with three solid carbide drills of the same geometry, but with different diameters. Investigation of cutting force parameters is a topic with constant research interest [23,24]. The aim of this study is to develop a mathematical model, with the employment of RSM and 3D FEM, for prediction purposes of the thrust force induced during Al7075-T6 drilling under commonly used conditions. This way, time and resources-consuming experimental work can be minimized, as well as the computationally intensive simulation runs. In order to do so, an investigation of the generated thrust forces and chip formation evolution was realized. Additionally, a comparison between the numerical and the experimental results was performed for validation. The proposed methodology ensures that the prediction model can be verified in a cost and time effective way, so that it can be used within the limits of this study.

2 Material and methods

2.1 Experimental setup

During the experimental stage of this research, three drills of the same grade (Kennametal KC7325) were used with

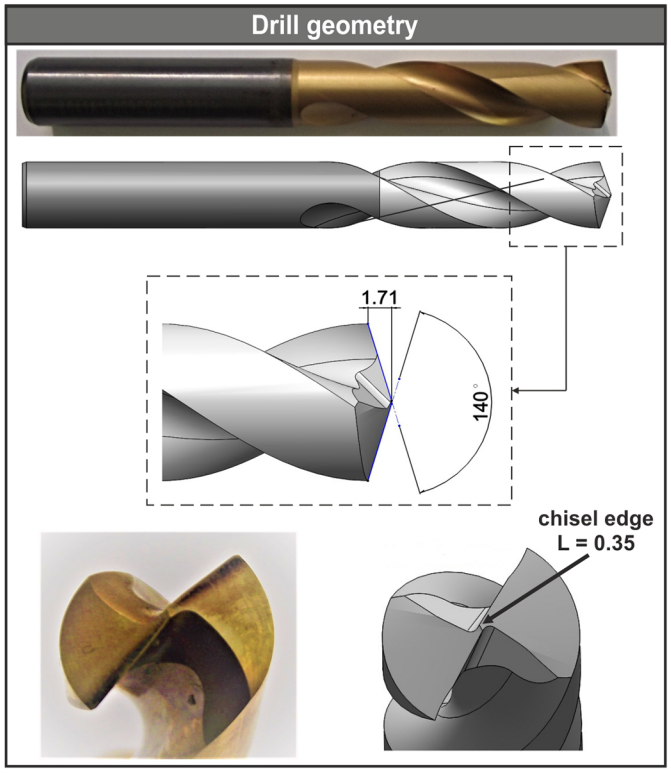

Fig. 1. Geometry parameters for the B041A10000CPG drill.

8 mm, 10 mm and 12 mm diameter respectively. These drills (B041A series) are solid carbide that consist of 10% cobalt and have double coating; a multilayer of TiN/TiAlN with 3.5 micron thickness and an outer layer of TiN with 15 micron thickness. Figure 1 illustrates the CAD model of the Ø10 drill compared to the physical model. The catalogue numbers for reference of the used drills are: B041A08000CPG (8 mm), B041A10000CPG (10 mm) and B041A12000CPG (12 mm).

A plate of Al7075-T6 with dimensions 150 mm × 130 mm × 15 mm served as the workpiece for the experiments that were carried out at three different cutting speeds (50 m/min, 100 m/min, 150 m/min) and three different feeds (0.15 mm/rev, 0.2 mm/rev, 0.25 mm/rev). The cutting conditions were chosen according to the manufacturer's recommended limits for Al7075-T6 alloy with respect to the drill diameters. Thus, the combination of the aforementioned parameters and the three drills used, led to a setup of 27 experiments (each tool was used to drill nine holes on the plate). In order to accurately perform the drilling tests, a HAAS (California, USA) VF1 CNC machining center and a BT40 cone were used. Additionally, a Kistler (Winterthur, Switzerland) type 9257B 3-component dynamometer was used for measuring the developed thrust forces. A typical measuring chain with data acquisition system (Kistler type 5697A1 with 16-bit resolution) was used in order to capture the measurements and store them, with the aid of a three-channel charge amplifier and DynoWare type 2825A software, to a desktop computer for analysis. The sampling rate was set to approximately 10 kHz, based on the specifications of the

Table 1. Basic mechanical and thermal properties of Al7075-T6 [25,26].

Mechanical properties					
Young's modulus	Density	Poisson's ratio	Hardness (HV)	Yield strength	Tensile strength
71.7 GPa	2810 kg/m^3	0.33	175	503 MPa	572 MPa
Thermal properties					
Heat capacity		Thermal expansion		Thermal conductivity	
0.960 J/g°C		2.2 × 10^{-5} μm/m°C		41.7 W/mK	

data acquisition system and the mean value of the measured thrust forces was used as the acquired data for easier comparison with the simulated values (see Sect. 3.1). Semi-synthetic oil-based coolant (KOOLrite 2270) was delivered to the tool throughout the whole experimental process. Table 1 contains the most important mechanical and thermal properties of the workpiece material and Figure 2 illustrates the workflow of this project. First stage includes the experimental setup (CNC and dynamometer setup), the execution of the designed experiments and the acquisition of the thrust force. Second stage includes the setup of the numerical model and the implementation of the simulations. Finally, third stage involves the analysis and validation of the results.

2.2 3D finite element model setup

2.2.1 Workpiece model setup

The 3D cutting simulations of the drilling processes were performed in the same order than the experiments with DEFORM3D^{TM} ver. 11.3 simulation software, on a desktop computer with dual-core CPU, 16GB RAM and SSD technology hard drive. In some of the simulations, the drill bit was allowed to fully penetrate the workpiece so that the full thrust force diagram can be acquired. However, most of the simulations were stopped when the thrust forces achieved steady state to save time. Depending on the time step applied, steady state occurred at a different point for each simulation. The time step was calculated based on the drill diameter and cutting speed used in each simulation. For example, the 10 mm tool at 100 m/min cutting speed rotates with 3183 min^{-1} or 53.05 s^{-1} according to equation (1), hence the tool completes one full rotation in 0.0189 s. Finally, the time step can be determined by dividing the previously calculated time value with the number of steps of the tool per revolution (360 steps), thus the time step for this case is 5.24×10^{-5} s. As a rule of thumb, the number of steps during drilling simulation should be close to 360 so that the tool can rotate one degree per step [27]. This way, it is ensured that the simulation will complete in a reasonable time period and, at the same time, yield acceptable results. It is possible though, to use an increased number of steps for an improved accuracy at the cost of very long simulation times

$$V_c = \frac{\pi D N}{1000}, \quad (1)$$

Where V_c is the cutting speed in m/min, D is the tool diameter in mm and N is the spindle speed in min^{-1}.

The workpiece was modelled to be circular and thin, with a thickness of about the radius of the drill for simplification purposes, but not thinner as it would be difficult for the workpiece to support the force of the drill and separation of the nodes would occur in a non-chip forming process according to Gardner and Dornfeld [28]. In addition, a center drill spot with regard to the drill point angle was made on the workpiece (Fig. 3a).

The purpose of this design is to significantly improve the simulation time, firstly because the removal of the material on the spot by the tool can be skipped and secondly because one revolution of the drill can take many time steps [28]. Three similar workpieces were used, but with different sizes, according to each drill geometry (see Tab. 1). All three workpieces were modelled as plastic with a mesh of tetrahedral elements that have four nodes. Depending on the dimensions of each workpiece, the mesh size varied. However, the minimum element size of the mesh was always 50% of the feed, based on the suggestion of DEFORM3D^{TM} [27]. A finer mesh was localized at the center of the workpiece in order to improve the fidelity at the contact interface. A ratio of 10:1 was used with this mesh, so that the total number of elements could be optimized. Even though a finer mesh usually yields more accurate results, the simulation time increases dramatically. Figure 3b depicts the tool-workpiece setup for the Ø10 mm drill.

2.2.2 Drill model setup

To model the drills, only their tips were used for simplification purposes. The drill tips were modelled as rigid with a mesh of approximately 20,000 to 30,000 tetrahedral elements. Since the area of the drill that is in contact with the workpiece is at the tip, a finer mesh with a 4:1 ratio was used at the tip (Fig. 3d). An adaptive remeshing technique was implemented so that more elements were generated in areas where there were large strains and strain rates, high temperatures and large deformations. The default strain and strain rate gradient were used. This technique further improves the simulation time and the produced chip geometry.

2.2.3 Boundary conditions and movement controls

The side of the workpiece was fixed in all positions (X, Y and Z), so that the velocity of all nodes is zero (Fig. 3c).

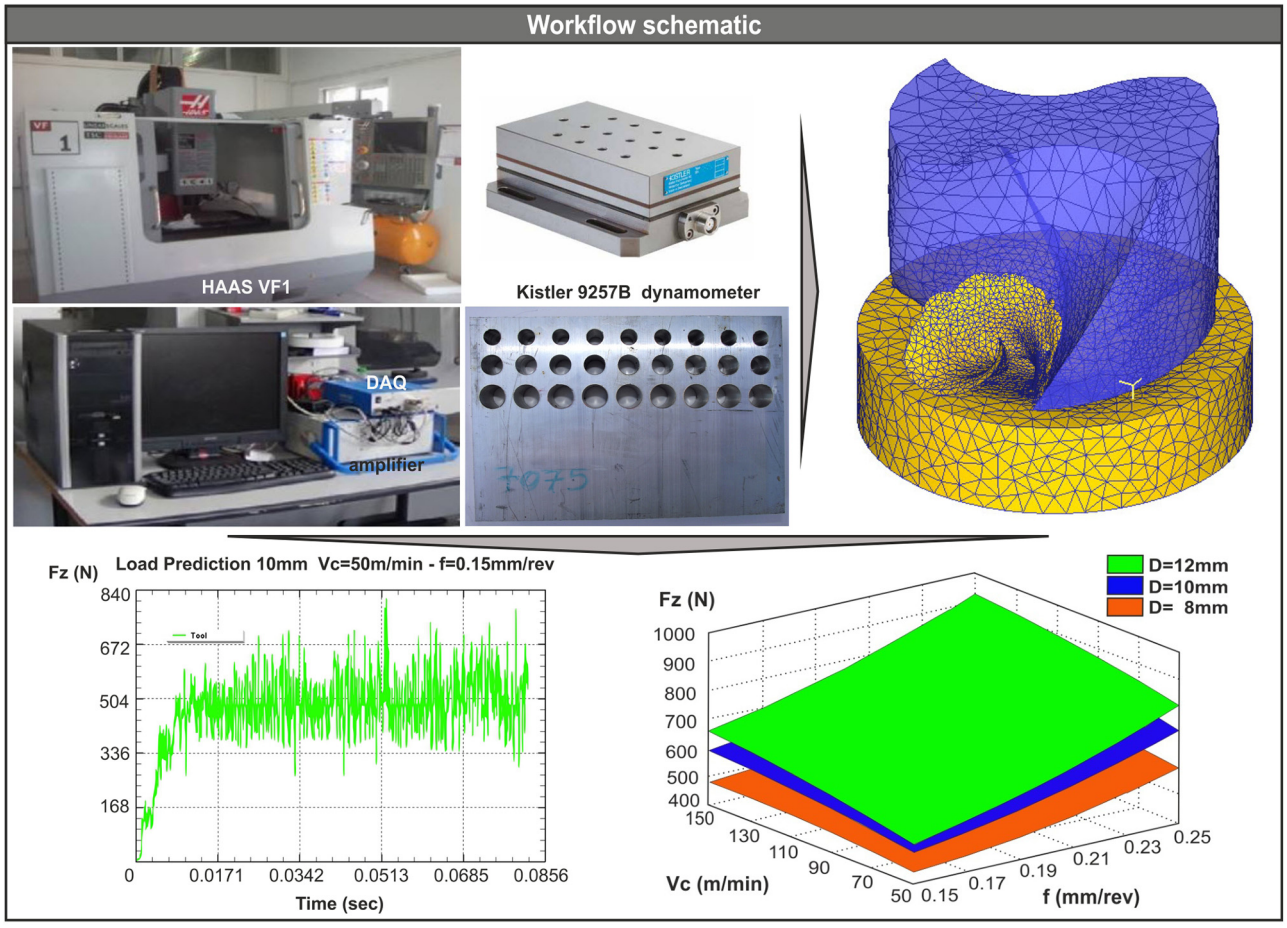

Fig. 2. The workflow of the drilling experiments and simulations.

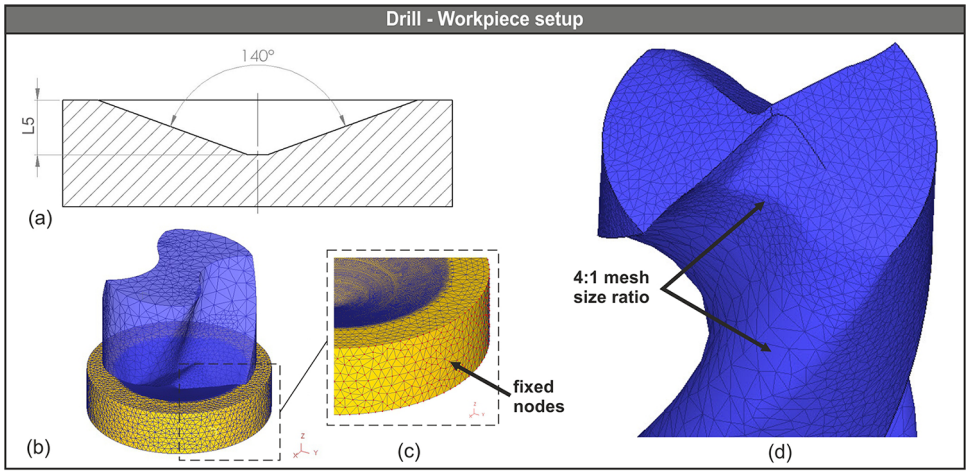

Fig. 3. Workpiece section (a), tool-workpiece setup (b), workpiece nodes (c) and drill model mesh (d).

In addition, heat exchange (with the environment) boundary conditions were assigned to all surfaces of the workpiece. To better approximate heat transfer through convection between the workpiece and the drill surface, a convection coefficient for oil based coolant with value of $2\,\mathrm{N}/(\mathrm{s}\times\mathrm{mm}\times{}^{\circ}\mathrm{C})$ was used [27], whereas for heat transfer through conduction in the tool-workpiece interface, a coefficient with the default value of $45\,\mathrm{N}/(\mathrm{s}\times\mathrm{mm}\times{}^{\circ}\mathrm{C})$ was used. Finally, a master-slave contact relationship was set for the workpiece and the generated chips, because it is most likely that the chips touch the workpiece. To define the rotational and translational movement of the drill, it was set to rotate around Z axis and move along Z axis (feed towards $-$Z) accordingly.

Table 2. Johnson − Cook constitutive model constants for Al7075-T6 [29].

A (MPa)	B (MPa)	C	n	m	T_0 (°C)	T_m (°C)
546	678	0.024	0.71	1.56	20	635

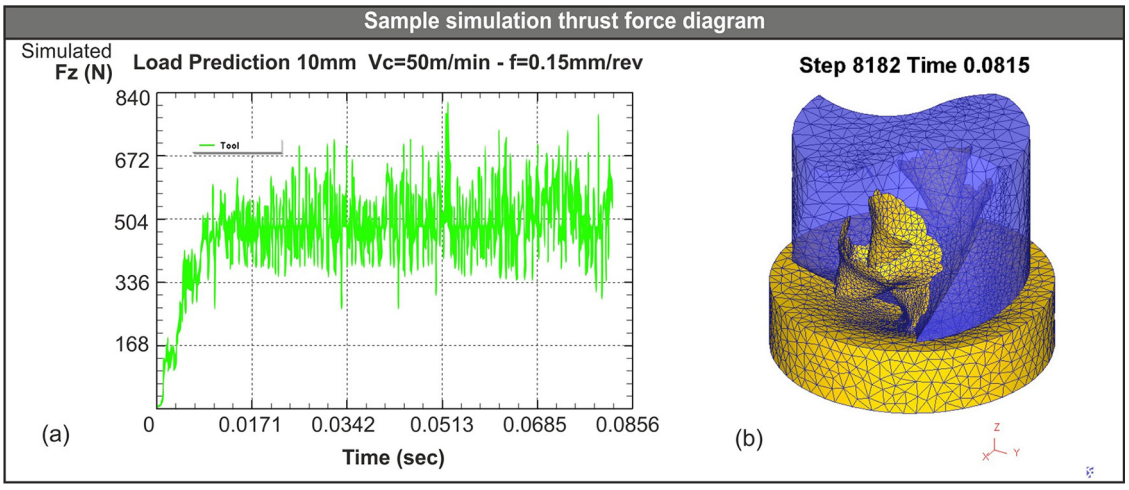

Fig. 4. The simulated thrust forces versus time diagram for the 10 mm tool (a) and the formed chip (b).

2.2.4 Material model setup

In order to simulate the flow stress of the Al7075-T6 alloy during the drilling operation, the generalized Johnson-Cook model was used. This model is widely used for stress analysis in deformations involving high strain, strain rate and temperature, and can be described by equation (2).

$$\sigma = (A + B\varepsilon^n)\left(1 + C\ln\frac{\dot{\varepsilon}}{\dot{\varepsilon}_0}\right)\left[1 - \left(\frac{T - T_0}{T_m - T_0}\right)^m\right], \quad (2)$$

where A is the initial yield stress, B is the strain hardening modulus, C is the strain rate dependence coefficient, ε is the plastic strain, n is the strain hardening exponent, m is the thermal softening coefficient, $\dot{\varepsilon}$ is the plastic strain rate, $\dot{\varepsilon}_0$ is the reference plastic strain rate, T is the reference temperature, T_0 is the bulk temperature and T_m is the melting temperature of the workpiece material. Since this constitutive model is commonly used for numerical studies of metal machining, the material constants of this model have been determined for a wide variety of workpiece materials. The material constants for Al7075-T6 alloy are presented in Table 2. In this study, a reference strain rate of 1/s was used.

The damage model used during this study was the normalized Cockcroft and Latham model in order to simulate the occurrence of material separation, when certain criteria are met. This model is defined as a function of the maximum principal stress σ' normalized with the effective stress $\overline{\sigma}$ [30].

As for the interaction between tool − chip interface, a hybrid model [21] was used for friction. To approximate the frictional stresses around the tool tip, where a more sticking behavior occurs, the shear friction model was used which can be determined by equation (3). This relationship is based on the assumption that the frictional stress is proportional to the shear strength of the weaker of the two materials that are in contact [31].

$$\tau_f = k_\tau \frac{\sigma_y}{\sqrt{3}} \quad (3)$$

where τ_f is the frictional stress, k_τ is a constant and σ_y is the uniaxial yield stress for the material.

In order to describe friction across the sliding zone, the Coulomb's friction model was used. This model is a good estimation for the sliding friction region and uses a constant μ, such that the frictional stress is determined by equation (4).

$$\tau_f = \mu\sigma_n \quad (4)$$

where τ_f is the frictional stress, μ is the friction coefficient and σ_n is the normal stress along the tool − chip interface.

For this study, the constant shear friction coefficient is $m = 0.7$ and the constant Coulomb friction coefficient is $\mu = 0.6$.

3 Results and discussion

3.1 Thrust force evaluation

Figure 4a illustrates a sample thrust force diagram obtained from the simulated drilling process of Al7075-T6 with a solid carbide 10 mm tool at cutting speed of $V_c = 50$ m/min and feed rate of $f = 0.15$ mm/rev. This diagram indicates that the produced thrust force increases

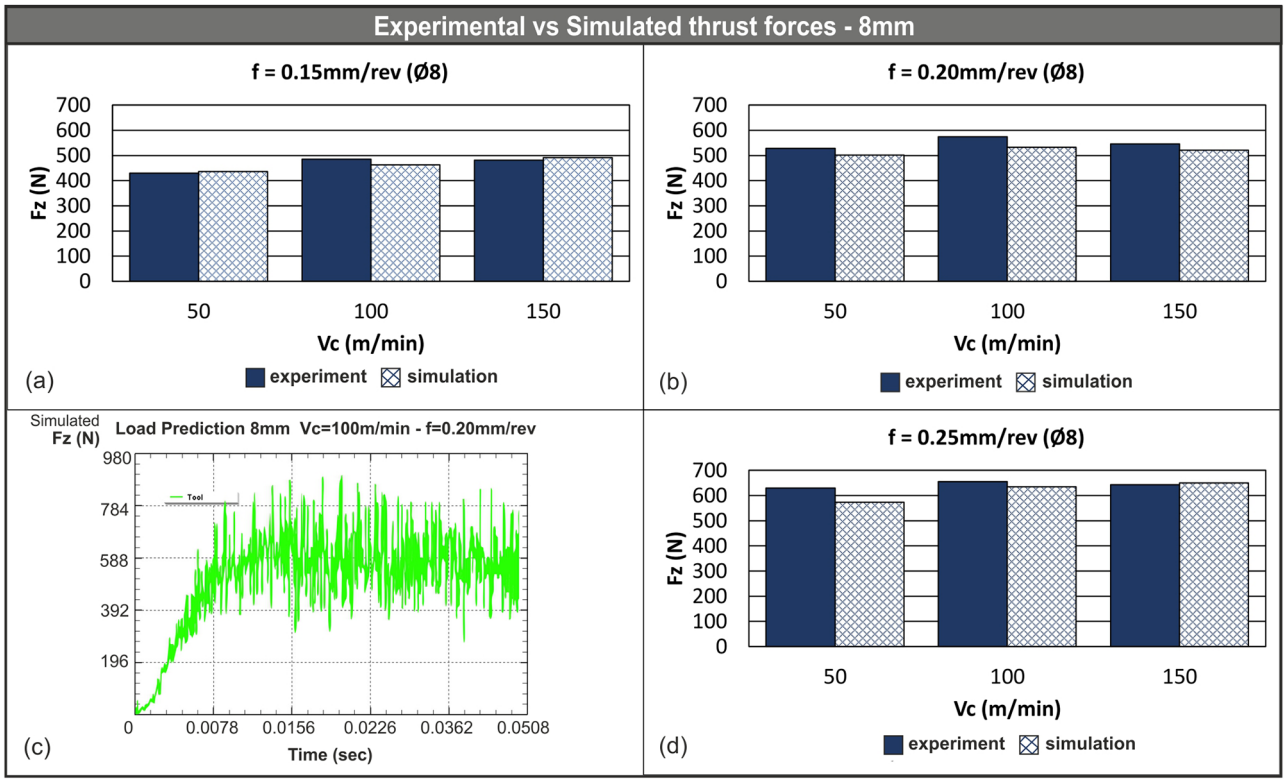

Fig. 5. Experimental versus numerical values of thrust force for the 8 mm drill with varied feed (a), (b), (d) and a sample force-time diagram (c).

rapidly, as soon as chisel's edge starts to press down the surface of the workpiece. Then quickly reaches a steady state, just before 0.0171 s thrust force stops to increase any further and maintains a steady state until the simulation was halted. The produced values of the simulated thrust force for each time step, after the steady state occurred, were used to plot the force-time graphs (Figs. 4a, 5c, 6c and 7c). As shown in Figure 4a, thrust forces fluctuated between 370 and 605 N for the majority of the simulation steps, with a mean value of about 500 N. Figure 4b depicts the produced chip after 8182 steps or 0.0815 s. The aforementioned tendency was observed in all the numerical tests that were performed. In order to eliminate any excessive or non-realistic values of thrust forces that were generated during the remeshing process on the workpiece, the default exponential smoothing (first order) of DEFORM3D™ was implemented.

The processing of the results shows in general a good agreement between the experimental and the numerical results. Figure 5 depicts the comparison between the experimental and the simulated mean values of the produced thrust forces for all nine possible combinations of cutting speed and feed for the 8 mm tool, in addition, a sample thrust force diagram from this set of simulations is depicted (Fig. 5c); it is shown that thrust force increases quickly until approximately 0.0078 s and then stabilizes at a mean value of around 530 N. Relative error between −5% and +2% is found in most of the experiments of this set. In the next cases, between the one with cutting speed of $V_c = 50$ m/min and feed of $f = 0.15$ mm/rev (Fig. 5a) and the one with $V_c = 150$ m/min and feed of $f = 0.25$ mm/rev (Fig. 5d) the relative error is approximately +1%, which is the lowest in the set. On the other hand, the maximum deviation between the experimental and the numerical results occurred in the simulation with cutting speed of $V_c = 100$ m/min and feed of $f = 0.20$ mm/rev (Fig. 5b), as well as with $V_c = 50$ m/min and $f = 0.25$ mm/rev (Fig. 5d). The relative error for these cases is −11% and −9% respectively.

In this set of simulations (8 mm tool), the standard deviation for the thrust force values was found to be between 15 and 142 N. Few cases in this set exhibited similar values of standard deviation and the average standard deviation for the set is close to 62 N. Moreover, the standard deviation for the simulation with cutting speed of $V_c = 50$ m/min and feed of $f = 0.15$ mm/rev (Fig. 5a) was found to be around 15 N, which is the lowest for all sets. In addition, the maximum standard deviation, of about 142 N, was calculated for the simulation with $V_c = 150$ m/min and $f = 0.25$ mm/rev (Fig. 5d).

Results of thrust forces for the 10 mm drill are also in good accordance with the equivalent experimental results. Figure 6 contains the three comparison graphs for the experimental and the simulated mean values of the produced thrust forces for the 10 mm tool and a sample thrust force diagram (Fig. 6c) that indicates the fast increase of thrust force to the point of 0.0089 s followed by a steady state. Mean value of thrust force for the given conditions is around 650 N. Moreover, the percentages of agreement between the experimental and the numerical

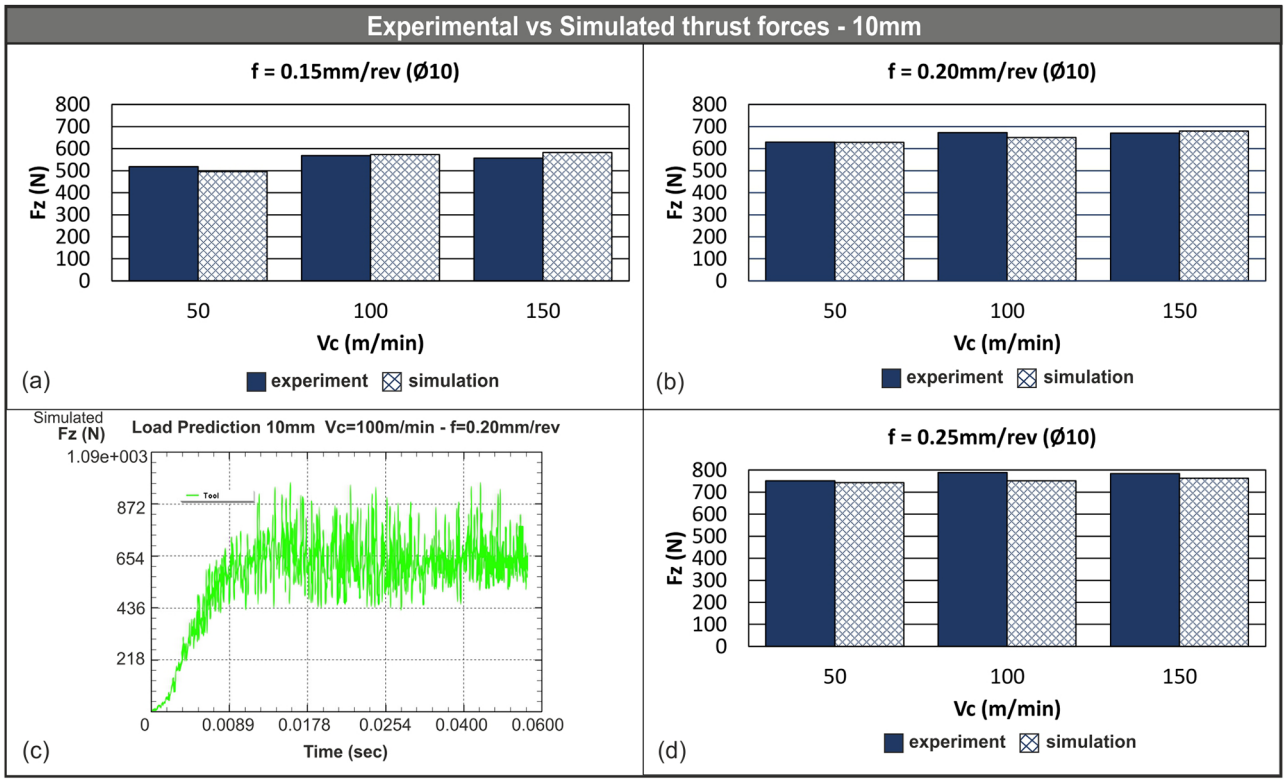

Fig. 6. Experimental versus numerical values of thrust force for the 10 mm drill with varied feed (a), (b), (d) and a sample force-time diagram (c).

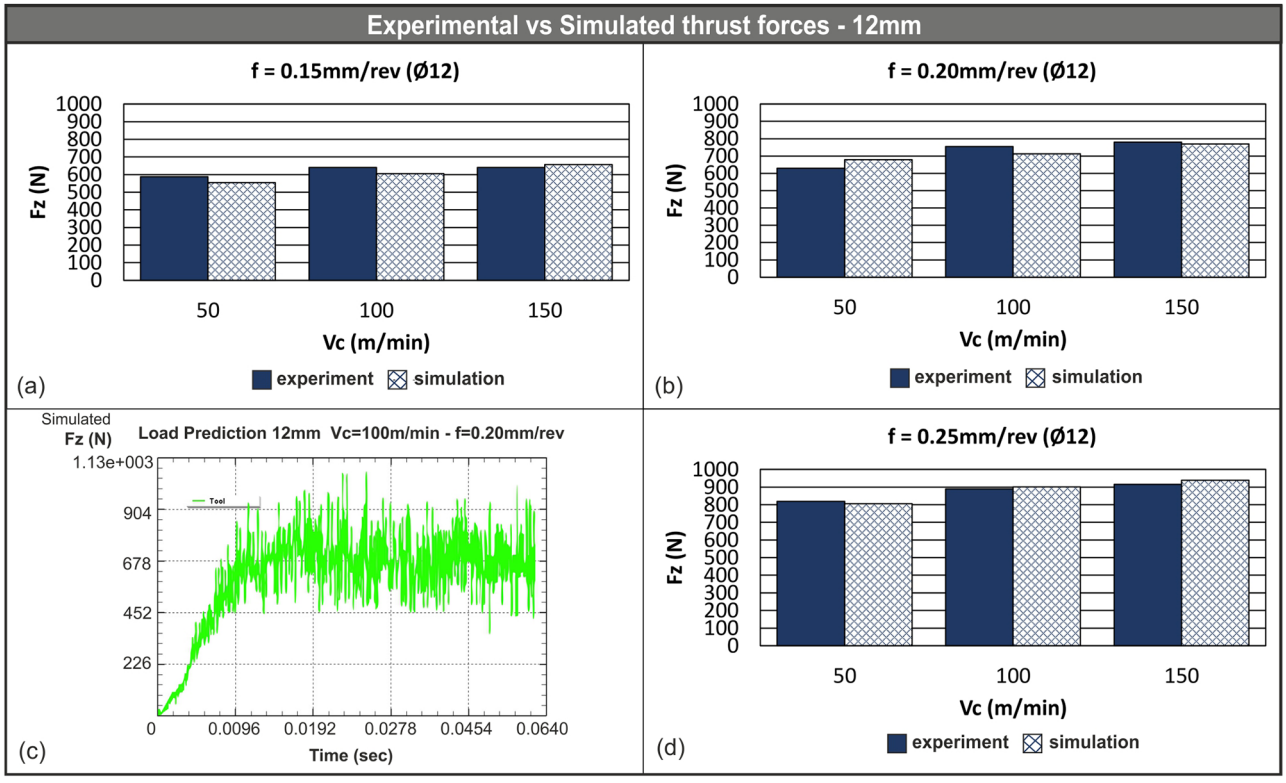

Fig. 7. Experimental versus numerical values of thrust force for the 12 mm drill with varied feed (a), (b), (d) and a sample force-time diagram (c).

results for each combination of cutting conditions tend to fluctuate less, compared to the set of results for the 8 mm drill. Relative error between −4% and +2% constitutes the majority for this set, and in some cases the correlation was close to 99% (cases with cutting speed of $V_c = 50$ m/min and feed of $f = 0.20$ and 0.25 mm/rev − Fig. 6b, d). The maximum deviation between the experimental and the numerical results in this set was found in the simulation with a cutting speed of $V_c = 100$ m/min and a feed of $f = 0.25$ mm/rev (Fig. 6d).

The standard deviation for the thrust force values of each of the simulations for the 10 mm tool, after the first order exponential smoothing, fluctuated between 20 and 75 N with an average value of 52 N. Simulation run with cutting speed of $V_c = 50$ m/min and feed of $f = 0.15$ m/min (Fig. 6a) displayed the lowest value for the set, whereas the simulation with cutting speed of $V_c = 50$ m/min and feed of $f = 0.25$ mm/rev displayed the highest standard deviation (Fig. 6d).

The relative error between the experimental and the numerical values of thrust forces for the results of the last set of simulations (12 mm drill), fluctuated between −6% and +8%. The comparison between the experimental and the numerical results for the thrust forces of all nine simulations in this set is illustrated in Figure 7. The sample thrust force diagram of Figure 7c points out the rapid increase of thrust force until 0.0096 s and the following steady state. Mean value of thrust force for the given conditions is approximately 710 N. Two simulations in this set, the one with $V_c = 150$ m/min and $f = 0.20$ mm/rev (Fig. 7b) and the other with $V_c = 50$ m/min and $f = 0.25$ mm/rev (Fig. 7d) yielded the highest agreement percentage for the set at approximately 99%, which is the highest value of correlation that observed through the whole process of 27 simulations. Additionally, under cutting conditions with $V_c = 100$ m/min and $f = 0.25$ mm/rev (Fig. 7d) the relative error slightly exceeds +1% (simulated value is marginally higher than experimental). Despite this fact, the maximum deviation was found to be in the case with a cutting speed of $V_c = 50$ m/min and a feed of $f = 0.20$ mm/rev (Fig. 7b), which is one of the highest for all the 27 simulations.

The standard deviation for the thrust forces in this set of simulations (12 mm tool) showed values between 50 and 119 N, with most cases yielding values close to 85 N. The lowest standard deviation was found to be approximately 50 N for cutting conditions with cutting speed of $V_c = 150$ m/min and feed of $f = 0.15$ mm/rev (Fig. 7a). On the other hand, the highest value of standard deviation was calculated to be around 119 N for the simulation with $V_c = 50$ m/min and $f = 0.25$ mm/rev (Fig. 7d).

It is worth mentioning that in three cases with cutting speed of $V_c = 150$ m/min, the experimental values of thrust forces were found to be slightly lower compared to the values for $V_c = 100$ m/min. Two of the three cases refer to drilling with the 8 mm tool at a feed of $f = 0.20$ and 0.25 mm/rev respectively, and one case to the drilling with the 10 mm tool at $f = 0.15$ mm/rev as observed in Figures 5b, 5d and 6a. In addition, four cases with $V_c = 150$ m/min display no fluctuation in generated thrust forces compared to the values found with $V_c = 100$ m/min. These cases are: 8 mm tool with $f = 0.15$ mm/rev, 10 mm tool with $f = 0.20$ and 0.25 mm/rev respectively and 12 mm tool with $f = 0.15$ mm/rev.

Figures 8a, 8c and 8e illustrate the variation of the experimental thrust forces with feed for varying tool diameter at certain cutting speed. Similarly, Figures 8b, 8d and 8f depict the variation of simulated values. It is obvious that both feed and cutting speed play an important role to the produced thrust forces, regardless of the tool diameter, especially the feed. There is a small but steady increase in thrust forces as cutting speed increases for each feed value and all tool diameters. Similarly, a noticeable and constant increase in thrust forces is present as feed increases for each cutting speed. For instance, according to figure 8b for the 12 mm tool, simulated thrust forces increase from approximately 550 N to 680 N and finally to 810 N at cutting speed of $V_c = 50$ m/min for each value of feed (0.15, 0.20 and 0.25 mm/rev respectively). The same linear trend applies for the other two tools. However, it is noted that thrust forces for the 8 mm tool increase at a different proportion.

As cutting speed increases, it is clear that simulated thrust forces increase for each value of feed in a similar manner. This pattern is different to the linearity that exists at cutting speed $V_c = 50$ m/min and is displayed mostly at $V_c = 100$ and 150 m/min (Fig. 8d and f). For example, with the 8 mm tool at $V_c = 100$ m/min (Fig. 8d) thrust forces increase from approximately 460 N to 510 N and finally to 630 N for each value of feed (0.15, 0.20 and 0.25 mm/rev). Additionally, for the same tool at $V_c = 150$ m/min (Fig. 8f) the increase pattern is similar, from 490 N to 520 N and then to 650 N.

3.2 Evolution of chip formation

Both the experimental and the simulated results indicate that the produced chip retains the same conical shape on each simulation regardless of the combination of the feed and cutting speed. However, the size of the chip (diameter of the conical shape chip) depends on the drill diameter. This is anticipated due to the fact that a larger flute can remove more material and thus produce wider chips. In general, the size of the flutes is related to the size of the drill.

Figure 9a depicts the evolution of the generated simulated chip during drilling of Al7075-T6 with a 10 mm, two flute twist drill, at 50 m/min cutting speed and 0.15 mm/rev feed rate, whereas Figure 9b illustrates the produced experimental chip for the same cutting conditions.

3.3 Mathematical modelling of thrust force

Since the correlation between the experimental and the numerical results was found to be very high on all three tools, a mathematical model is possible so that future experiments for different drill diameters and similar cutting conditions can be skipped. The proposed mathematical model for thrust force was developed with the aid of RSM, which is a proven statistical methodology that provides excellent experiment design and result presentation. There are cases in literature where researchers in the field of machining have successfully implemented RSM in

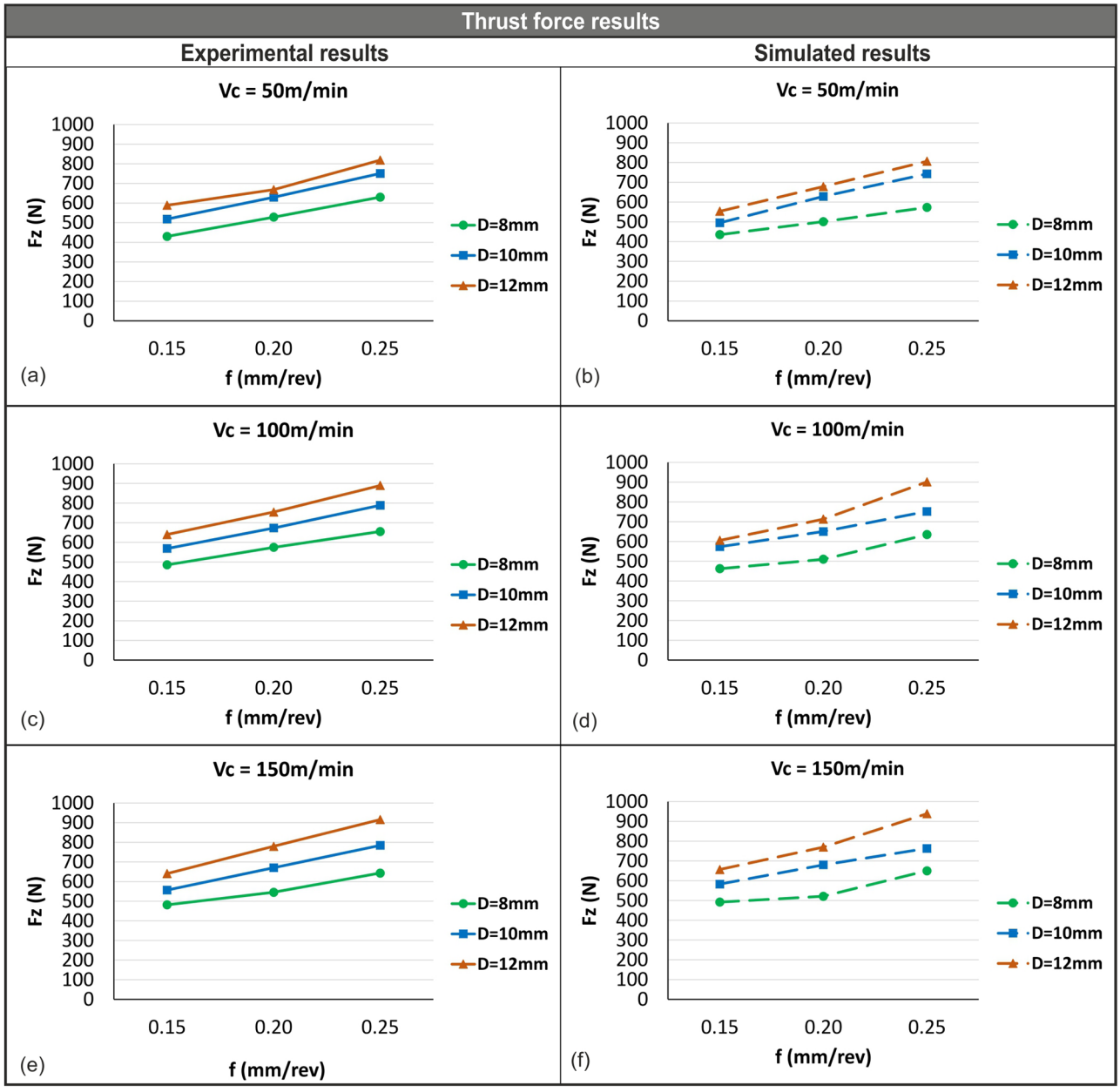

Fig. 8. Variation of the experimental (a), (c), (e) and the numerical (b), (d), (f) values of thrust force with feed for varying tool diameter.

their research [22,32–35] with excellent results, thus the use of RSM was selected for this study. Because this research includes 27 drilling experiments and simulations, the mathematical modelling was performed with a full factorial design in mind, based on the numerical results. Table 3 illustrates the design of experiments and the corresponding output for the numerical study.

The first step that was made during modelling was to fit the regression model. Based on the number of factors (drill diameter, cutting speed and feed) that were involved in the numerical study, the fitted model that occurred is a second order polynomial with linear, quadratic and interactive terms. Equation (5) represents the second order polynomial for this study.

$$Y = b_0 + b_1X_1 + b_2X_2 + b_3X_3 + b_4X_1^2 + b_5X_2^2 + b_6X_3^2 + b_7X_1X_2 + b_8X_1X_3 + b_9X_2X_3 \quad (5)$$

where Y is the response of the model, thus the thrust force in this case, X_i are the coded values of the model (drill diameter, cutting speed and feed) and b_i are the regression coefficients that depend on the number of factors of the model (three in this case).

Using the aforementioned polynomial and the data that are presented in Figures 5–7, the complete mathematical model based on the verified simulated results that was

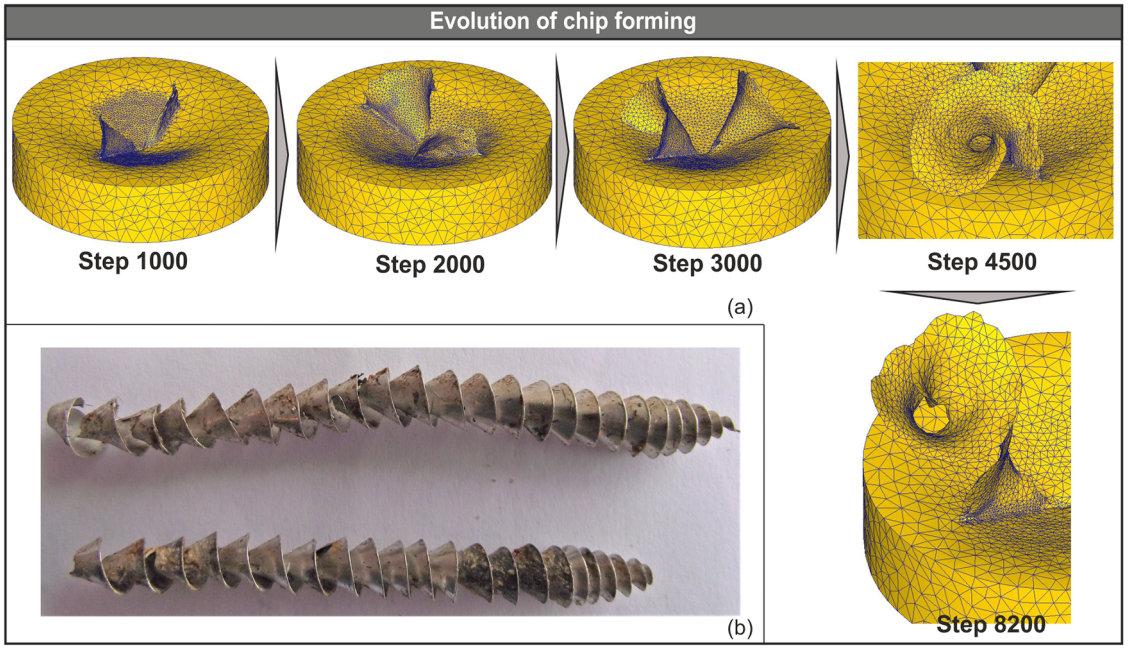

Fig. 9. The evolution of the simulated chip (a) and the experimental one (b) for the 10 mm drill.

Table 3. Design of experiments.

Std order	D (mm)	V_c (m/min)	f (mm/rev)	$F_{z\ \text{simulated}}$ (N)
1	8	50	0.15	435.6
2	8	50	0.20	501.4
3	8	50	0.25	573.5
4	8	100	0.15	462.5
5	8	100	0.20	510.3
6	8	100	0.25	634.9
7	8	150	0.15	491.5
8	8	150	0.20	520.8
9	8	150	0.25	649.8
10	10	50	0.15	495.9
11	10	50	0.20	628.8
12	10	50	0.25	742.9
13	10	100	0.15	573.5
14	10	100	0.20	650.4
15	10	100	0.25	751.6
16	10	150	0.15	582.4
17	10	150	0.20	679.9
18	10	150	0.25	763.0
19	12	50	0.15	553.8
20	12	50	0.20	612.9
21	12	50	0.25	806.7
22	12	100	0.15	605.8
23	12	100	0.20	713.2
24	12	100	0.25	901.3
25	12	150	0.15	656.5
26	12	150	0.20	770.0
27	12	150	0.25	938.7

Table 4. ANOVA results for thrust force.

Source	Degree of freedom	Sum of squares	Mean square	f-value	p-value
Regression	9	427676	47519.5	103.01	0.000
Residual error	17	7842	461.3		
Total	26	435518			
R-sq (adj) = 97.25%					
Term	PE coefficient	SE coefficient	t-value	p-value	
Constant	238	295	0.81	0.432	
D	79.5	46.1	1.73	0.102	
V_c	−0.21	1.06	−0.19	0.848	
f	−4797	1557	−3.08	0.007	
D^2	−5.52	2.19	−2.52	0.022	
V_c^2	−0.00451	0.00351	−1.29	0.215	
f^2	9883	3507	2.82	0.012	
$D \times V_c$	0.20	0.062	3.23	0.005	
$D \times f$	301.6	62.0	4.86	0.000	
$V_c \times f$	−0.56	2.48	−0.22	0.825	

developed, is represented by equation (6).

$$F_z = 238 + 79.5D - 0.21V_c - 4797f - 5.52D^2 - 0.00451V_c^2 + 9883f^2 + 0.2DV_c + 301.6Df - 0.56V_cf \quad (6)$$

where F_z is the thrust force in N, D is the drill diameter in mm, V_c is the cutting speed in m/min and f is the feed in mm/rev.

3.4 Analysis and validation of model

After fitting the model, analysis of variance (ANOVA) has been performed for validation purposes. During this step, a confidence level of 95% was used for all intervals. The adjusted R-squared for this model found to be as high as 97.25% proving the validity of the fit. In addition, the high correlation can be proved by the p-values that are 0.05 and lower. Due to the fact that the significance level is 0.05, the contribution to the validity of the thrust force model according to Table 4 is done by these factors: f with a p-value of 0.007, D^2 with $p = 0.022$, f^2 with $p = 0.012$, $D \times V_c$ with $p = 0.005$ and $D \times f$ with $p = 0.000$.

Table 4 contains the sum of squares and degrees of freedom of the analysis. Sum of squares includes the sum of squared deviations due to each of the nine factors and the sum of squares due to error. Mean square is the ratio of sum of squares to the degree of freedom and the f-value is the ratio of mean square of regression model to the mean square of residual error. Lastly, the p-value of the analysis is 0.000 which means that the correlation is very high as the probability of getting an extreme result is very low.

The significance of the tool diameter D, cutting speed V_c and feed rate f is highlighted with the main effects plot (Fig. 10). As already pointed out with the aid of Figure 8, the key parameters that effect thrust forces are the tool diameter and the feed rate. More importantly, it is obvious that as diameter and feed increase, thrust forces also increases.

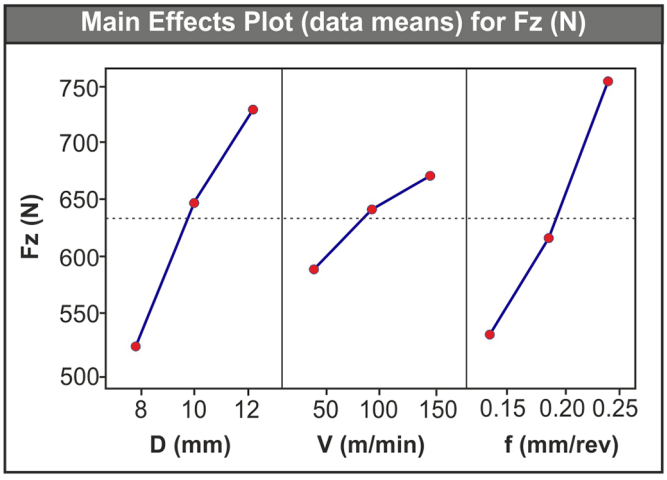

Fig. 10. Main effects plot for thrust force.

Following the validation of goodness of fit, the next step was the residual analysis to check the accuracy of the model. Figure 11 contains four graphs: the normal probability plot of the residuals (Fig. 11a), the residuals versus the fitted values (Fig. 11b), the distribution of error histogram (Fig. 11c) and the residuals versus the order of the data (Fig. 11d). The normality of distribution in all graphs suggests the validity of the regression analysis. Specifically, from the normal probability plot it is understandable that the errors follow an almost linear pattern which means that the errors follow a normal distribution pattern. The residuals versus the fitted values graph shows that the residuals are evenly scattered on both sides of the reference line of the graph, thus the variance is

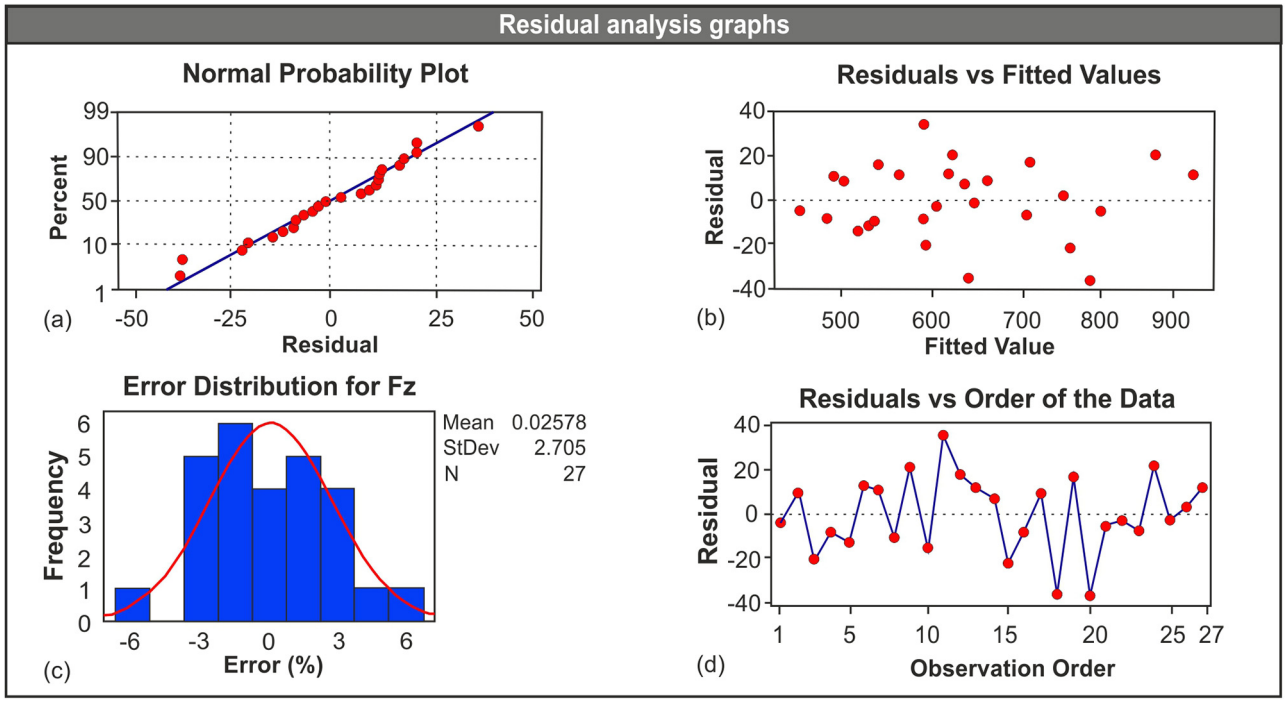

Fig. 11. Residual analysis graphs: probability plot (a), residuals versus fitted values (b), error histogram (c) and residuals versus order (d).

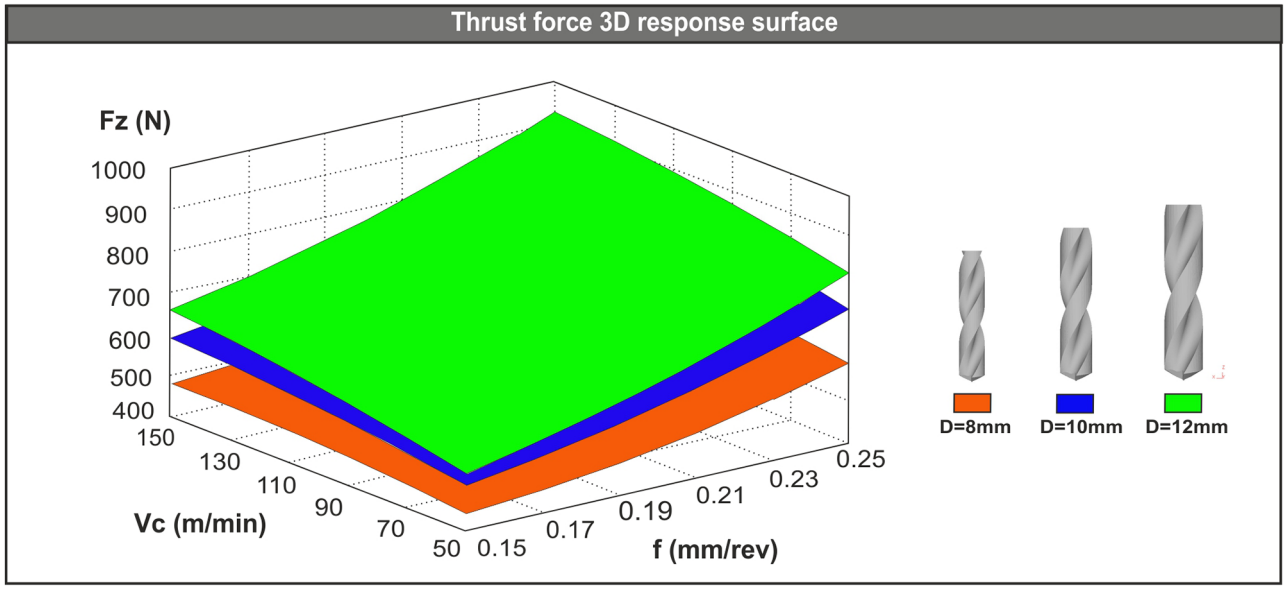

Fig. 12. 3D plots of the thrust force for each drill.

constant. In addition, the histogram depicts a normality in distribution between the error percentages. Finally, the residuals versus order graph indicates that there are no obvious systematic effects in the data due to time.

Final step of the mathematical modelling was the analysis of the developed prediction model. With the aid of 3D response surface plots, the combined effect of the tool diameter and cutting conditions on thrust forces were analyzed. Figure 12 illustrates the generated 3D surfaces for each drill diameter based on the polynomial solutions. The inputs of the polynomial are within the investigated range for cutting speed and feed, thus from 50 to 150 m/min for cutting speed and 0.15 to 0.25 mm/rev for feed. According to Figures 10 and 12 it is observed that:

– As a larger drill diameter is selected, the produced thrust force increases notably (the larger the diameter, the higher values of thrust force).

Table 5. Confirmation of mathematical model for F_z.

Set	Simulated F_z (N)	Predicted F_z (N)	Relative error (%)
I (8 mm)	487.6	483.1	−0.92
II (10 mm)	602.9	582.0	−3.47
III (12 mm)	611.5	636.6	4.11

– Similarly, at higher values of feed, the produced thrust force is significantly increased.
– On the other hand, any increase in cutting speed has limited effect (increase) on thrust force.

Eventually, to further validate the mathematical model, a set of three extra simulations (one for each drill) was performed for the prediction of F_z. The cutting conditions were selected arbitrarily from within the range of the experimental data. The selected conditions are: $V_c = 75$ m/min and $f = 0.18$ mm/rev. Table 5 includes the produced results which are deemed sufficient since the relative error for all three cases is below 5%.

4 Conclusions

The development of a prediction model for the generated thrust forces during drilling of Al7075-T6, with the aid of RSM and the implementation of 3D FEA, is presented in this study. A complete series of 27 3D simulations was carried out under different cutting conditions (speed and feed rate) in addition to the three different tool diameters that were used. The simulated results were validated via experiments and the correlation between the simulated and the experimental results exceeded 95% in most cases. After thoroughly analyzing the model for its accuracy (5.9%) and goodness of fit, it is concluded that the developed model can safely predict the thrust forces under certain limits that are discussed in this research. Moreover, the morphology of the produced chips during drilling of Al7075-T6 was introduced. Finally, through this analysis the following conclusions are drawn:

– Increase in tool diameter and feed rate leads to significant boost of thrust force. Specifically, an increase of close to 20% in thrust force is observed when changing to the 10 mm drill from the 8 mm one or when increasing the feed to 0.20 mm/rev from 0.15 mm/rev. The equivalent shift from 10 mm to 12 mm or from 0.20 mm/rev to 0.25 mm/rev amplifies F_z by more than 40% for both cases.
– On the other hand, any increase in cutting speed increases thrust force at a small but not negligible amount; a step-up from 50 m/min to 100 m/min was estimated to rise F_z approximately by 8.5%, whereas from 100 m/min to 150 m/min by 4%.
– The factors that affect the most the statistical model are: f, D^2, f^2, $D \times V_c$ and $D \times f$ since their p-values is lower than the significance level.
– The produced chips tend to maintain a conical shape, regardless of the cutting conditions, whereas the diameter of the curling of chip increases as larger tool diameter was selected.

Nomenclature

T_0	Bulk temperature of the workpice material (K)
V_c	Cutting speed (m/min)
D	Drill diameter (mm)
$\overline{\sigma}$	Effective stress (N/m^2)
f	Feed (mm/rev)
τ_f	Frictional stress at the tool − chip interface (N/m^2)
A	Initial yield stress (N/m^2)
σ'	Maximum principal stress (N/m^2)
T_m	Melting temperature (K)
σ_n	Normal stress (N/m^2)
ε	Plastic strain
$\dot{\varepsilon}$	Plastic strain rate (s^{-1})
$\dot{\varepsilon}_0$	Reference plastic strain rate (s^{-1})
T	Reference temperature (K)
m	Shear friction coefficient
μ	Sliding friction coefficient
N	Spindle speed (min^{-1})
B	Strain hardening modulus (N/m^2)
n	Strain hardening exponent
C	Strain rate dependence coefficient
m	Thermal softening coefficient for JC model
F_z	Thrust force (N)
σ_y	Uniaxial yield stress (N/m^2)

References

[1] B. Klamecki, Incipient Chip Formation in Metal Cutting – A Three Dimensional Element Analysis, Urbana-Champaign: University of Illinois, 1973
[2] Y.B. Guo, D.A. Dornfeld, Finite element modeling of burr formation process in drilling 304 stainless steel, J. Manuf. Sci. Eng. **122**, 4 (2000)
[3] M. Abouridouane, F. Klocke, D. Lung, Microstructure-based 3D finite element model for micro drilling carbon steels, Proc. CIRP **8** (2013)
[4] X. Nan, L. Xie, W. Zhao, On the application of 3D finite element modeling for small-diameter hole drilling of AISI 1045 steel, Int. J. Adv. Manuf. Technol. **84** (2016)

[5] P.J. Arrazola, T. Matsumura, A. Kortabarria, A. Garay, D. Soler, Finite element modelling of chip formation process applied to drilling of Ti64 alloy in: Proceedings of the 6th International Conference on Leading Edge Manufacturing in 21st Century: LEM 2011, J-Stage, 2011, pp. 1–6
[6] M. Asad, T. Mabrouki, H. Ijaz, M. Aurangzeb Khan, W. Saleem, On the turning modeling and simulation: 2D and 3D FEM approaches, Mech. Ind. **15**, 5 (2014)
[7] O. Isbilir, E. Ghassemieh, Finite element analysis of drilling of titanium alloy, Proc. Eng. **10** (2011)
[8] X. Gao, H. Li, Q. Liu, P. Zou, F. Liu, Simulation of stainless steel drilling mechanism based on Deform-3D, Adv. Mater. Res. **160–162**, (2011)
[9] A. Majeed, A. Iqbal, J.J. Lv, Enhancement of tool life in drilling of hardened AISI 4340 steel using 3D FEM modeling, Int. J. Adv. Manuf. Technol. **95** (2018)
[10] S.F. Miller, A.J. Shih, Thermo-mechanical finite element modeling of the friction drilling process, J. Manuf. Sci. Eng. **129**, (2007)
[11] J.P. Davim, C. Maranhão, Study on plastic strain and plastic strain rate in machining of steel AISI 1020 using FEM analysis, Mater. Des. **30**, 1 (2009)
[12] T. Belis, P. Kyratsis, A. Antoniadis, Stress Analysis on Twist Drill Tools Combining CAD based Methodology and Finite Element Analysis, NOVA Science Publishers, chapter **2**, pp. 31–42, 2013
[13] M. Lotfi, S. Amini, I.Y. Al-Awady, 3D numerical analysis of drilling process: heat, wear, and built-up edge, Adv. Manuf. **6** (2018)
[14] A.K. Parida, Simulation and experimental investigation of drilling of Ti-6Al-4V alloy, Int. J. Light Mater. Manuf. **1**, 3 (2018)
[15] M. Nagaraj, A.J.P. Kumar, C. Ezilarasan, R. Betala, Finite element modeling in drilling of Nimonic C-263 alloy using deform-3D, C − Comput. Model. Eng. Sci. **118**, 3 (2019)
[16] T. Dou, H. Fu, Z. Li, X. Ji, S.S. Bi, Prediction model, simulation, and experimental validation on thrust force and torque in drilling SiCp/Al6063, Int. J. Adv. Manuf. Technol. **103** (2019)
[17] J.R. Flachs, M. Salahshoor, S.N. Melkote, Mechanistic models of thrust force and torque in step-drilling of Al7075-T651, Prod. Eng. **8** (2014)
[18] E. Bahçe, B. Özdemir, Investigation of the burr formation during the drilling of free-form surfaces in al 7075 alloy, J. Mater. Res. Technol. **8**, 5 (2019)
[19] J.Y. Kao, C.Y. Hsu, C.C. Tsao, Experimental study of inverted drilling Al-7075 alloy, Int. J. Adv. Manuf. Technol. **102** (2019)
[20] J.P. Davim, C. Maranhão, M.J. Jackson, G. Cabral, J. Grácio, FEM analysis in high speed machining of aluminium alloy (Al7075-0) using polycrystalline diamond (PCD) and cemented carbide (K10) cutting tools, Int. J. Adv. Manuf. Technol. **39** (2008)
[21] İ. Ucun, 3D finite element modelling of drilling process of Al7075-T6 alloy and experimental validation, J. Mech. Sci. Technol. **30** (2016)
[22] N.K. Sahu, A.B. Andhare, Prediction of residual stress using RSM during turning of Ti-6Al-4V with the 3D FEM assist and experiments, SN Appl. Sci. **1** (2019)
[23] S.N. Grigoriev, M.A. Volosova, V.D. Gurin, A.Y. Seleznyov, Investigation of force parameters acting on a single cutting insert made of ceramics in face milling of hardened steel, Mech. Ind. **16**, 702 (2015)
[24] H. Aouici, M. Elbah, A. Benkhelladi, B. Fnides, L. Boulanouar, Comparison on various machinability aspects between mixed and reinforced ceramics when machining hardened steels, Mech. Ind. **20**, 109 (2019)
[25] MatWeb Material Property Data, https://www.matweb.com, Accessed: 29/11/2019
[26] E. Jafarzadeh, M.R. Movahhedy, S. Khodaygan, Prediction of machining chatter in milling based on dynamic FEM simulations of chip formation, Adv. Manuf. **6** (2018)
[27] Scientific Forming Technologies Corporation, DEFORM V11.3 (PC) Documentation, 2016
[28] J.D. Gardner, D. Dornfeld, Finite Element Modeling of Drilling Using DEFORM, Simulation (2006)
[29] N.S. Brar, V.S. Joshi, B.W. Harris, Constitutive model constants for Al7075-T651 and Al7075-T6, AIP Conf. Proc. **1195**, 945 (2009)
[30] M.G. Cockcroft, D.J. Latham, Ductility and the Workability of Metals, J. Inst. Met. **96** (1968)
[31] M. Agmell, Applied FEM of metal removal and forming − first edition, Studentlitteratur, Lund, 2018
[32] S. Kosaraju, V.G. Anne, Optimal machining conditions for turning Ti-6Al-4V using response surface methodology, Adv. Manuf. **1** (2013)
[33] P. Kyratsis, C. Garcia-Hernandez, D. Vakondios, A. Antoniadis, Thrust Force and Torque Mathematical Models in Drilling of Al7075 Using the Response Surface Methodology in: J.P. Davim (ed.), Design of Experiments in Production Engineering, Springer International Publishing, Cham 2016, pp. 151–164
[34] P. Kyratsis, A. Markopoulos, N. Efkolidis, V. Maliagkas, K. Kakoulis, Prediction of thrust force and cutting torque in drilling based on the response surface methodology, Machines **6**, 2 (2018)
[35] W. Frifita, S. Ben Salem, A. Haddad, M. Athmane Yallese, Optimization of machining parameters in turning of Inconel 718 Nickel-base super alloy, Mech. Ind. **21**, 2 (2020)

Cite this article as: A. Tzotzis, C. García-Hernández, J.-L. Huertas-Talón, P. Kyratsis, FEM based mathematical modelling of thrust force during drilling of Al7075-T6, Mechanics & Industry **21**, 415 (2020)